KSME

Springer

Journal of Mechanical Science and Technology 35 (3) 2021

Original Article
DOI 10.1007/s12206-021-0232-x

Keywords:
· Axial ultrasonic-assisted grinding
· Brittle fracture
· Grinding force and grinding force ratio
· Subsurface damage

Correspondence to:
Yanyan Yan
yyy@hpu.edu.cn;
Yafei Zhang
zhangyf727@foxmail.com

Citation:
Yan, Y., Zhang, Y., Zhao, B., Liu, J. (2021). Surface formation and damage mechanisms of nano-ZrO_2 ceramics under axial ultrasonic-assisted grinding. Journal of Mechanical Science and Technology 35 (3) (2021) 1187~1197. http://doi.org/10.1007/s12206-021-0232-x

Received April 19th, 2020
Revised November 18th, 2020
Accepted November 30th, 2020

† Recommended by Editor Hyung Wook Park

Surface formation and damage mechanisms of nano-ZrO_2 ceramics under axial ultrasonic-assisted grinding

Yanyan Yan, Yafei Zhang, Bo Zhao and Junli Liu

School of Mechanical and Power Engineering, Henan Polytechnic University, Jiaozuo 454003, Henan, China

Abstract In this study, the surface formation and damage mechanism of hard-brittle materials in axial ultrasonic-assisted grinding (AUAG) were revealed using the grinding force and grinding force ratio. Theoretical analysis presented that the grinding force and grinding force ratio in AUAG are relatively small. AUAG is a machining method with a large tangential force and a small normal force, which can promote the removal of hard-brittle materials and reduce the surface and subsurface damage (SSD). Scratching and grinding tests of nano-ZrO_2 ceramics were conducted to validate the theoretical analysis. The results demonstrated that the periodic tangential force under the AUAG promotes the nucleation and propagation of shallower lateral micro-cracks, thereby allowing the easier removal of hard-brittle materials. Additionally, the proportion of brittle fracture was less, and the surface roughness and maximum SSD depth were significantly small. Therefore, AUAG is a suitable ultra-precision machining technique for hard-brittle materials.

1. Introduction

Nano-ZrO_2 ceramics exhibit excellent mechanical and physical properties such as heat temperature resistant, wear resistance and corrosion resistance; therefore, they have widespread applications in aerospace, automotive, engineering machinery, biomedical, and other fields [1, 2]. However, they are hard–brittle materials with poor machining performance due to high hardness and low fracture toughness [3]. Therefore, machining defects, including micro-cracks and residual stress, frequently occur during the conventional grinding (CG) of nano-ZrO_2 ceramics [4]. In particular, the severe subsurface damage (SSD) that occurs in machined surfaces significantly affects the performance and service lives of components. Therefore, it is crucial to improve the surface quality and reduce the degree of SSD during the precision and ultra-precision machining of nano-ZrO_2 ceramics. Researchers have done a lot of work on how to improve the surface quality in grinding processes [5]. Talon et al. [6] formulated a new corrosion inhibitor (V-active VCI) and analyzed the effect of AISI 4340 steel using aluminum oxide grinding wheel under the different cutting fluid. The results showed that the cutting fluid with corrosion inhibitor was beneficial for the average roughness. In the recently, ultrasonic-assisted grinding (UAG) is considered as a highly suitable grinding method for processing ceramic materials, when compared with CG; it can effectively reduce both the grinding force and grinding heat as well as improve surface quality [7, 8]. Uhlmann et al. [9] found that the introduction of axial ultrasonic vibrations modified the formation mechanism of a machined surface during creep feed grinding and increased the overlap of adjacent abrasive tracks, which is beneficial for improving the subsurface quality. Liang et al. [10, 11] determined that compared to CG, axial UAG (AUAG) significantly reduces the SSD depth and can yield a higher grinding surface quality. Liu et al. [12] studied the relationship between cutting force and the maximum undeformed chip thickness (UCT) of brittle materials in rotary ultrasonic machining, and established a cutting force model. Experimental results show that the theoretical model can be used to predict the relationship between input variables and cutting forces. Zhang et al. [13] performed

an ultrasonic-assisted scratch test (UAST) on C-plane sapphire. The experimental results show that the UAST can effectively reduce the scratch loads and inhibit the propagation of micro-cracks as well as improve the plastic removal rate. Li et al. [14] studied the material removal mechanism and grinding force of SiC ceramics in UAG processing based on the varied-depth nano-scratch test and the grain trajectory during UAG. Baraheni et al. [15] investigated the generation of SSD in rotary ultrasonic-assisted face grinding under ductile deformation and brittle fracture. Their research indicated that UAG reduced the SSD depth by 30 % compared to CG. Wang et al. [16] established the theoretical models of grinding force and material removal rate for UAG, and revealed the reasons that UAG reduces grinding force and improves surface quality. Yang et al. [17] found that the introduction of ultrasonic vibrations effectively reduced the grinding force during the grinding of ZrO_2 ceramics and prolonged the service life of the grinding wheel. Although studies on the grinding mechanism of hard–brittle materials in UAG have advanced significantly, most research regarding the surface formation and damage mechanisms of hard-brittle materials primarily focus on the toughness processing methods, and similar investigations of the brittleness processing methods have not progressed.

Hence, the material removal mechanism of nano-ZrO_2 ceramics in AUAG based on brittleness was analysed in terms of the grinding force and grinding force ratio. Subsequently, combined with the comparative grinding test of nano-ZrO_2 ceramics, the mechanisms of material formation and surface damage in AUAG were analysed to promote the practical application of AUAG in ultra-precision machining of hard–brittle materials.

2. Mechanism of material removal in AUAG

For this study, the following were assumed: (1) the particles are completely rigid cones and are uniformly distributed along the circumference of the grinding wheel; (2) the average contact stress between the particles and the machined surface is F_p; (3) the amplitude and frequency remain unchanged during AUAG.

2.1 Kinematics analysis of a single particle in AUAG

The cutting motion model of AUAG is displayed in Fig. 1. The workpiece is subjected to high-frequency ultrasonic vibrations along the Y-axis direction (frequency f, amplitude A), to undergo AUAG. According to the model shown in Fig. 1(a), the cutting path of a single particle during AUAG can be expressed by Eq. (1).

$$\begin{cases} x(t) = v_w t + R\sin(\omega_s t) \\ y(t) = A\sin(\omega t + \varphi) \\ z(t) = R - R\cos(\omega_s t) \end{cases} \tag{1}$$

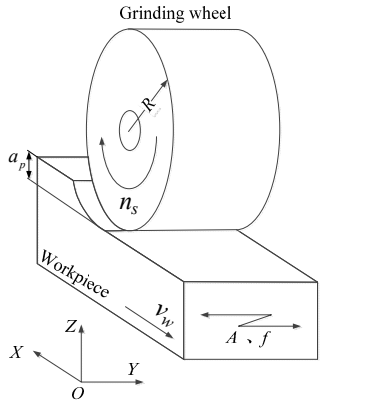

(a) The cutting motion model

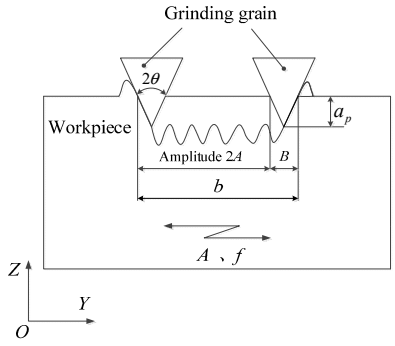

(b) The grinding width

Fig. 1. Cutting model of AUAG.

where v_w is the feed rate (m/min), R is the grinding wheel radius (mm), ω_s is the grinding wheel angular speed (rad/s), i.e., $\omega_s = 2\pi n_s$ (where n_s is the rotation speed of grinding wheel), ω is the angular frequency of the workpiece (rad/s), i.e., $\omega = 2\pi f$, and φ is the initial phase of the ultrasonic vibration (rad), assuming $\varphi = 0$.

Based on Eq. (1), the relative velocity of a single particle is expressed by Eq. (2), and the relative acceleration of a single particle is expressed by Eq. (3).

$$\begin{cases} v_x(t) = v_w + \omega_s R\cos(\omega_s t) \\ v_y(t) = A\omega\cos(\omega t) \\ v_z(t) = \omega_s R\sin(\omega_s t) \end{cases} \tag{2}$$

$$\begin{cases} a_x(t) = -\omega_s^2 R\sin(\omega_s t) \\ a_y(t) = -A\omega^2\sin(\omega t) \\ a_z(t) = \omega_s^2 R\cos(\omega_s t) \end{cases} . \tag{3}$$

Using Eq. (2), the cutting track length of a single particle during AUAG (l_s) can be expressed as follows:

$$\begin{aligned} l_s &= \int_0^t \sqrt{v_x(t)^2 + v_y(t)^2 + v_z(t)^2}\, dt \\ &= \int_0^t \sqrt{v_w^2 + 2v_w \cdot \omega_s R\cos(\omega_s t) + (\omega_s R)^2 + (2A\pi f\cos(2\pi ft))^2}\, dt \end{aligned} . \tag{4}$$

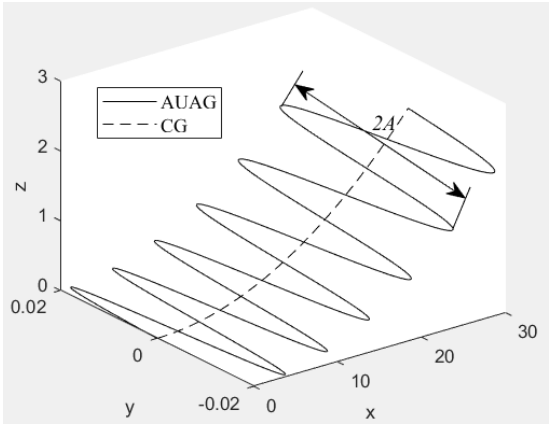

Fig. 2. The simulation of cutting track of a single particle.

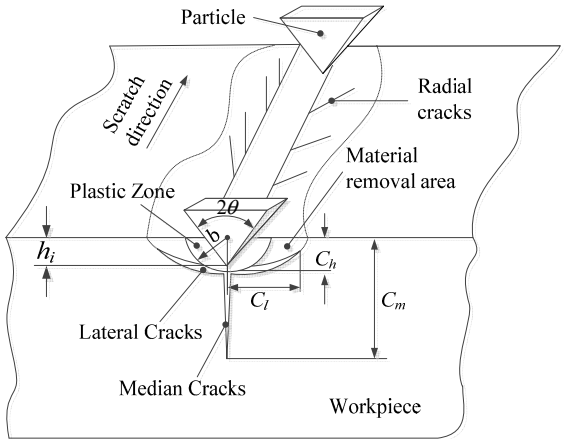

Fig. 3. Material removal process during single-grit scratching.

In addition, according to Fig. 1(b), the grinding width of a single particle (b) in AUAG can be expressed as follows:

$$b = B + 2|A|\sin(2\pi ft) = 2\left[a_p \tan\theta + |A|\sin(2\pi ft)\right] \quad (5)$$

where a_p is the grinding depth (mm), and θ is the half–apex angle of particle.

Based on the kinematics analysis of AUAG, the movement trajectory can be obtained by MATLAB (simulation parameters: f = 20 kHz, A = 20 μm, n_s = 1450 r/min, R = 200 mm, v_w = 0.6 m/min). The simulation results are presented in Fig. 2.

According to the simulation results, compared to CG, in AUAG, the grinding width of a single particle is wider and the cutting track is longer and presents a regular sinusoidal trajectory along the axis of the grinding wheel. This will cause the cutting tracks between adjacent grains to interfere with each other, which is conducive to reducing the size of the abrasive debris.

2.2 Analysis of material removal mechanism

During the grinding process, the UCT is an important parameter index to characterize the material removal mechanism. Therefore, the UCT in the AUAG process is analysed first. It is also assumed that hard–brittle materials are removed by brittle fracture because the grinding depth in this study is greater than the critical depth of the ductile-to-brittle transition. The material removal process in single-grit scratching is illustrated in Fig. 3. The depth of the lateral crack (C_h) and the depth of the median crack (C_m) in AUAG can be expressed as follows [18]:

$$C_h = \left[\frac{3(1-2v)}{5-4v} + \frac{2\sqrt{3}}{\pi(5-4v)}\frac{E}{\sigma_y}\cot\theta\right]^{1/2}\tan\theta \cdot h_i \quad (6)$$

$$C_m = 0.206\frac{(E\cdot H_V)^{1/3}}{(K_{ID}\cdot\beta)^{2/3}}(\cot\theta)^{4/9}(\tan\theta)^{4/3}\cdot(h_i)^{4/3} \quad (7)$$

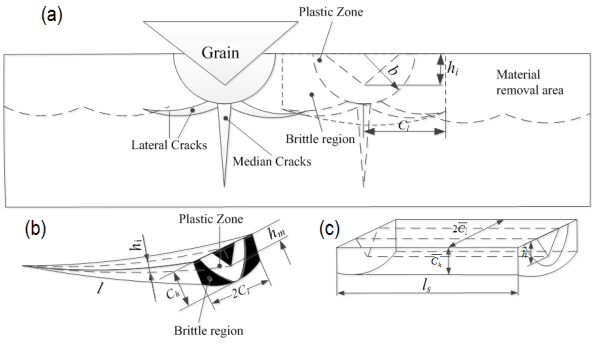

Fig. 4. Material removal volume of a single particle: (a), (b) the theoretical volume of the material removal; (c) the equivalent volume of the material removal.

where E is the elastic modulus, υ is Poisson's ratio, σ_y is the yield stress, h_i is the UCT, K_{ID} is the dynamic fracture toughness, and K_{ID} = 0.3 K_{IC} (where K_{IC} is the static fracture toughness), H_V is Vickers hardness, and β is the material parameter determined by elastic recovery.

Considering the influence of the intersections between lateral cracks, the material removal volume (*MRV*) can be approximated as a quadrangular pyramid, as depicted in Fig. 4. According to Fig. 4(b), the *MRV* of a single particle per unit time (V_g) in the AUAG process can be expressed as follows:

$$\begin{aligned} V_g &= \frac{1}{3}\cdot(2C_l\cdot C_h)\cdot l_s = \frac{1}{3}\cdot\left(2\cdot\frac{1}{7}\cdot C_m\cdot C_h\right)\cdot l_s \\ &= \frac{2}{21}\cdot\left\{\left[\frac{3(1-2v)}{5-4v} + \frac{2\sqrt{3}}{\pi(5-4v)}\frac{E}{\sigma_y}\cot\theta\right]^{1/2}\tan\theta\right\} \\ &\quad\cdot\left\{0.206\frac{(E\cdot H_V)^{1/3}}{(K_{IC}\cdot\beta)^{2/3}}(\cot\theta)^{4/9}(\tan\theta)^{4/3}\right\}\cdot h_i^{7/3}\cdot l_s \\ &= \frac{2}{21}\cdot\kappa\cdot h_i^{7/3}\cdot l_s \end{aligned} \quad (8)$$

where C_l is the length of a lateral crack, $C_l = 1/7\,C_m$ [19].

Furthermore, the maximum *MRV* of a single particle ($V_{g\text{-}max}$)

can be expressed as follows:

$$V_{g\text{-max}} = \frac{2}{21} \cdot \kappa \cdot h_{\text{m}}^{7/3} \cdot l_s \tag{9}$$

where h_m is the maximum UCT.

According to Eq. (9), the theoretical volume of the material removal per unit time (MRV_S) by the wheel can be expressed by Eq. (10).

$$MRV_s = N_d V_{g-\max} = \frac{2\kappa}{21}(N \cdot v_s \cdot b) \cdot h_m^{7/3} \cdot l_s \tag{10}$$

where v_s is the linear velocity of grinding, N_d is the dynamic distribution density of the grains per area, and N is the number of active grains per area.

Simultaneously, the theoretical volume of the material removal per unit time (MRV_w) of the workpiece can be expressed as follows:

$$MRV_w = v_w \cdot (a_p \cdot b) \ . \tag{11}$$

As the actual grinding width of the AUAG process becomes wider, the material removal rate (MRR) increases. Equating (MRV_s) with (MRV_w), the maximum UCT of a single particle in AUAG can be obtained as Eq. (12).

$$h_m = \left(\frac{21 a_p \cdot v_w}{2\kappa \cdot N \cdot v_s l_s}\right)^{3/7} . \tag{12}$$

The surface formation mechanisms of hard–brittle materials are a synchronous mechanism of brittleness and toughness. When the maximum UCT is less than the critical depth of toughness removal, the material is mainly removed by the mechanism of toughness; otherwise this occurs according to the mechanism of brittleness. It can be seen form Eq. (12) that the maximum UCT of a single particle in AUAG is significantly reduced because of the interference between adjacent abrasive particles. Therefore, the material removal volume based on the removal modes of toughness is larger and the workpiece surface quality is improved.

The UCT varies with the grinding depth, which is inconvenient for the study of the grinding force. Therefore, the MRV is considered to be equivalent to a quadrangular prism, as presented in Fig. 4(c). According to Figs. 4(b) and (c), the relationship between the maximum UCT (h_m) and the average UCT ($\bar{h}$) can be expressed by Eq. (13).

$$\bar{h} = \frac{\sqrt{3}}{3} h_m = \frac{\sqrt{3}}{3} \left(\frac{21 a_p \cdot v_w}{2\kappa \cdot N \cdot v_s l_s}\right)^{3/7} . \tag{13}$$

2.3 Model of grinding force in AUAG

According to Zhao et al. [20], the grinding force in CG can be expressed as follows:

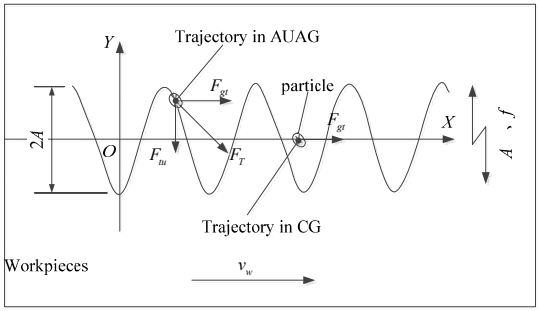

Fig. 5. Tangential grinding force model of a single particle.

$$\begin{cases} F_{gt} = F_{tc} + F_{ts} \\ F_{gn} = F_{nc} + F_{ns} \end{cases} \tag{14}$$

where F_{gt} and F_{gn} are the tangential and normal grinding forces under CG, respectively, F_{tc} and F_{nc} are the tangential and normal forces generated by the cutting deformation, respectively, F_{ts} and F_{ns} are the tangential and normal forces produced by friction, respectively.

According to the superposition principle of mechanics, the grinding force in AUAG is composed of the grinding force in CG and the periodic pulse force generated by the ultrasonic vibration, as displayed in Fig. 5. Based on Fig. 5, the grinding force in AUAG can be expressed by Eq. (15).

$$\begin{cases} F_T = F_{gt} + F_{tu} \\ F_N = F_{gn} + F_{nu} \end{cases} \tag{15}$$

where F_T and F_N are the tangential and normal grinding forces in AUAG, respectively, F_{tu} and F_{nu} are the tangential force and the normal force of the periodic pulse force, respectively.

The grinding forces generated by the cutting deformation and friction can be expressed by Eqs. (16) and (17), respectively [20].

$$\begin{cases} F_{tc} = \dfrac{\pi}{4} F_P (\bar{h})^2 \sin\theta \\ F_{nc} = F_P (\bar{h})^2 \sin\theta \tan\theta \end{cases} \tag{16}$$

$$\begin{cases} F_{ts} = \mu \delta \bar{p} \\ F_{ns} = \delta \bar{p} \end{cases} \tag{17}$$

where F_P is the main cutting force acting on a unit cutting area (N/mm^2), δ is the top area of a particle (mm^2), μ is the friction coefficient, and $\bar{p}$ is a constant for the average contact pressure between the worn surface and the workpiece, $\bar{p} = 4 p_0 v_w / (d_s v_s)$, as determined experimentally.

Assuming that the equivalent mass of the ultrasonic vibration workpiece is M, the periodic pulse force of a single particle can be expressed as follows based on Newton's second law:

$$\begin{cases} F_{tu} = Ma_t / N_d = -(MAw^2 \sin wt) / v_s Nb \\ F_{nu} = Ma_n / N_d = 0 \end{cases} \tag{18}$$

where a_t and a_n are the tangential and normal accelerations generated by the axial ultrasonic vibration, respectively, i.e., $a_t = a_y(t)$ and $a_n = 0$.

According to Eqs. (15)-(18), the grinding force and grinding force ratio of a particle in AUAG can be expressed by Eqs. (19) and (20), respectively.

$$\begin{cases} F_T = \sqrt{(\frac{\pi}{4} F_P (\bar{h})^2 \sin\theta + \mu\delta\bar{p})^2 + ((MA\omega^2 \sin\omega t) / v_s Nb)^2} \\ F_N = F_P (\bar{h})^2 \sin\theta \tan\theta + \delta\bar{p} \end{cases} \tag{19}$$

$$K_F = \frac{F_N}{F_T} = \frac{F_P (\bar{h})^2 \sin\theta \tan\theta + \delta\bar{p}}{\sqrt{(\frac{\pi}{4} F_P (\bar{h})^2 \sin\theta + \mu\delta\bar{p})^2 + ((MA\omega^2 \left|\sin\omega t\right|) / v_s Nb)^2}} . \tag{20}$$

It can be seen from Eq. (19) and Fig. 5 that the grinding force in AUAG is smaller than that in CG, owing to the decrease in the average UCT. In addition, it is also found that the tangential grinding force in AUAG keeps continuously varying in the vibration cycle under the influence of a pulse action. This is because the tangential grinding force in AUAG is based on the superimposition of that in CG and the periodic pulse force. Moreover, according to Eq. (20), the grinding force ratio (K_F) in the AUAG process is also significantly smaller than that in CG, owing to the periodic pulse cutting force. Therefore, AUAG is a machining method with a large tangential force and a small normal force, which is helpful for the removal of a hard–brittle material and reduces the surface damage and SSD. This is because the small normal grinding force can reduce the brittle fracture of a machined surface, thereby improving the surface integrity. Moreover, the periodic tangential force in AUAG can effectively increase both the nucleation rate and extension degree of lateral cracks, which is conducive to the formation of numerous lateral micro-cracks on the grinding surface, which thus, promotes the removal of hard–brittle materials. Therefore, AUAG can improve the surface integrity of hard–brittle materials and is a suitable processing method for them.

3. Experimental verification

Based on the theoretical model, scratching tests of nano-ZrO_2 ceramics in AUAG were performed to verify the material removal mechanisms. The type of nano-ZrO_2 ceramic used in this experiment was the Yttria-stabilized zirconia (YSZ), which was provided by Jiaozuo Weina Technology Co., Ltd. The primary mechanical properties of nano-ZrO_2 ceramics are listed in Table 1. The nano-ZrO_2 specimen used in the test was a rectangular block (10 mm×15 mm×5 mm).

Table 1. Material properties of nano-ZrO_2 ceramic specimen.

Properties	Value
Density (g/cm^3)	5.5-6.05
Elastic modulus (GPa)	220
Poisson's ratio	0.3
Bending strength (MPa)	1100
Fracture toughness K_{IC} (MPa · m$^{1/2}$)	12
Compressive strength (MPa)	2500

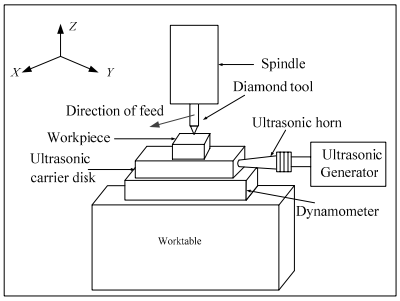

(a) Scratching illustration

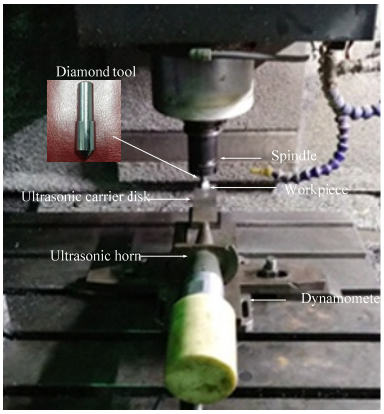

(b) Scratching site

Fig. 6. Nano-ZrO_2 ceramic scratch test device.

The scratching test was conducted with a vertical machining centre (VMC850E, Zhongjie), whose specific performance parameters are listed in Table 2. The experimental site is presented in Fig. 6. Common scratching (CS) and axial ultrasonic-assisted scratching (AUAS) were performed when the ultrasonic generator was turned off and on, respectively. The ultrasonic frequency used in the experiment is the resonance frequency of the horn, and its value is 20.325 kHz. The single factor test was designed as summarized in Table 3. The grinding force in the test was measured by a grinding force data acquisition system, comprising a dynamometer (9257B, Kistler), a charge amplifier (5070A), a data acquisition card (5679A), the Labview software, and a computer. The scratched grooves on the machined surface were observed using ultra-depth microscope and white light interferometer (TALYSDRFCC1, Tay-

Table 2. Vertical machining centre parameters (Zhongjie VMC850E).

Properties	Parameters
Displacement X, Y, Z (mm)	850, 500, 540
Power (kW)	7.5/11
Spindle speed (r/min)	50-8000
Spindle maximum torque (N·m)	35.8

Table 3. Scratch test parameter settings.

Group no.	v_w(mm / min)	a_p (μm)	A(μm)
1	10/20/30/40/50	10	10
2	40	5/10/15/20/25	10
3	40	10	4/6/8/10/12

Fig. 7. The picture of white light interferometer.

lor Hobson). The white light interferometer used in the experiment is shown in Fig. 7.

The grinding test was also conducted with the ultra-precision surface grinder (GTS-6016AHD) to analyze the surface and subsurface quality in AUAG. A resin-based diamond-grinding wheel used in the test. The abrasive size of the grinding wheel is 270#; the dimensions of the grinding wheel is ∅355× 35×∅127 , and the linear velocity of grinding v_s was taken as 26.95 m/s. Grinding test site is shown in Fig. 8. CG and AUAG were performed when the ultrasonic generator was turned off and on, respectively. The single factor grinding test was designed as summarized in Table 4. The SR was measured by TIME3221 surface roughness profiler. The form and depth of the SSD were studied using the section polishing method. The machined surface was polished before the measurement; subsequently, subsurface cracks were observed by scanning electron microscopy (Merlin Compact), and the SSD depth was measured.

Table 4. Grinding test parameter settings.

Group no.	v_w(m / s)	a_p (μm)	A(μm)
1	9/11/13/15/17	10	10
2	15	5/10/15/20/25	10
3	15	10	4/6/8/10/12

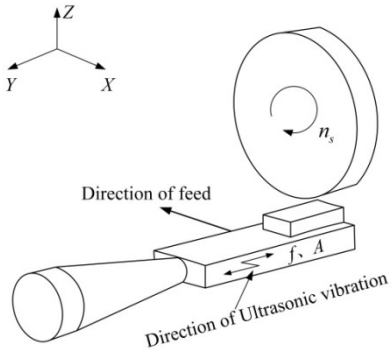

(a) Grinding diagram

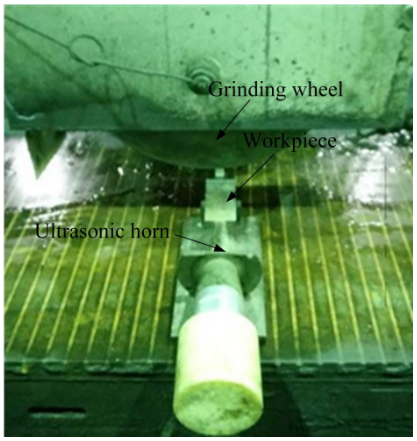

(b) Grinding test site

Fig. 8. Nano-ZrO_2 ceramic grinding test device.

4. Results and discussion

Based on the experimental results and the theoretical analysis, the grinding force, grinding force ratio, and surface formation and damage mechanisms in AUAG were analysed in detail.

4.1 Analysis of grinding force and grinding force ratio

The grinding force and grinding force ratio in the CS and AUAS tests are depicted in Fig. 9. According to Figs. 9(a) and (b), in the AUAS test, these properties are smaller than in the CS test under the same grinding parameters, and in both the CS and AUAS tests, they increase with both the feed rate and grinding depth. The former trend is because the cutting tracks of a single grain in the AUAS process are longer, which decreases the average UCT, and therefore, the grinding force in the AUAS test is comparatively smaller. Furthermore, the tan-

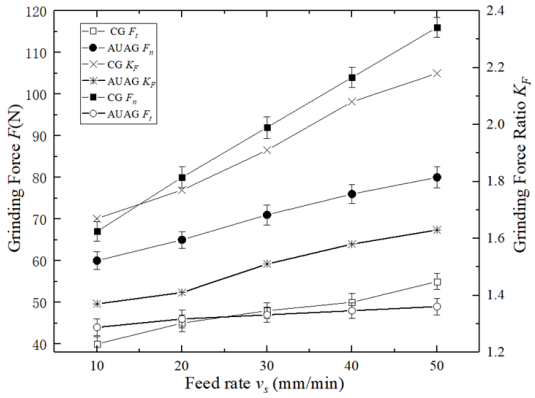

(a)

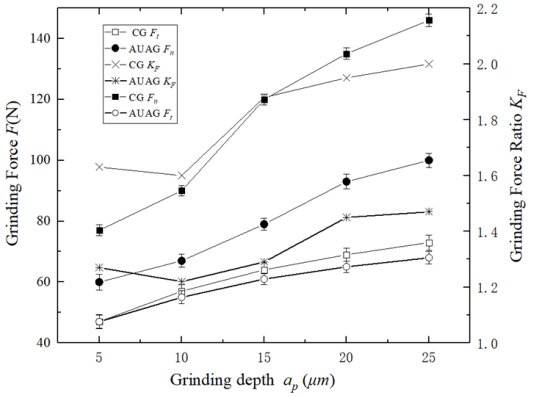

(b)

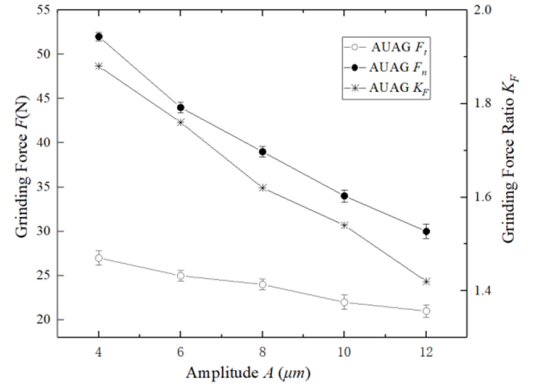

(c)

Fig. 9. The grinding force and grinding force ratio.

gential grinding force in the AUAS test is superimposed on the periodic pulse force, which leads to the reduction of the grinding force ratio. Therefore, the superposition of axial vibrations can promote the material removal and improve surface quality. In addition, because the average UCT increases with the feed rate and grinding depth, the grinding force and grinding force ratio in the both CS and AUAS tests increase versus both these properties.

It can be seen from Fig. 9(c) that the grinding force and grinding force ratio in the AUAS test decrease significantly with

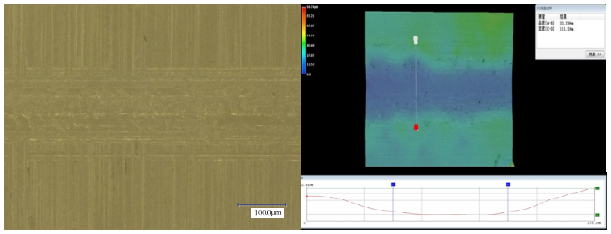

(a) CS (v_w = 40 mm/min, a_p = 10 μm)

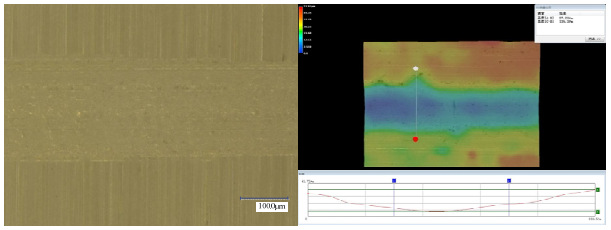

(b) AUAS (v_w = 40 mm/min, a_p = 10 μm, A = 10 μm)

Fig. 10. Surface profiles of the grooves.

the vibration amplitude. This is because the cutting track length and grinding width of a single grain increase with the vibration amplitude, which decreases the average UCT and increase the number of active grains, thereby leading to the above trend. On the other hand, the effect of axial vibrations is enhanced with the vibration amplitude, which can further promote the material removal. Therefore, the grinding force needed to remove the material decreases with the vibration amplitude.

4.2 Analyses of scratching morphology

Fig. 10 depicts the surface profiles under different scratching modes. It can be seen form Fig. 10 that the surface grooves in the AUAS tests are wide and shallow, and that the surface quality is significantly better than that in the CS test. This is because the ultrasonic vibration direction is perpendicular to the feed direction, and the tangential grinding force changes periodically under high-frequency vibration, which impacts both sides of the grooves; therefore, the actual grinding width of a single particle is wide. Moreover, the normal grinding force in the AUAS test significantly decreases; thus, the proportion of brittle fracture in the material removal process is reduced and the grooves are shallow.

Fig. 11 displays the scratching morphologies under different scratching modes. The groove surface in the AUAS is significantly smoother than that in the CS. This is because the periodic pulse force in the brittle removal mode can promote the formation of lateral micro-cracks on both sides of the groove, which facilitate the material removal process. Furthermore, the lateral micro-cracks intersect with each other, which reduce the chips size; thereby the surface in the AUAS is smoother than that in the CS. From Fig. 11, the damages of the scratch contour boundary in both the CS and AUAS are gradually intensified and the scratch grooves become significantly wider with the increase in the cutting depth. However, the phenomenon of

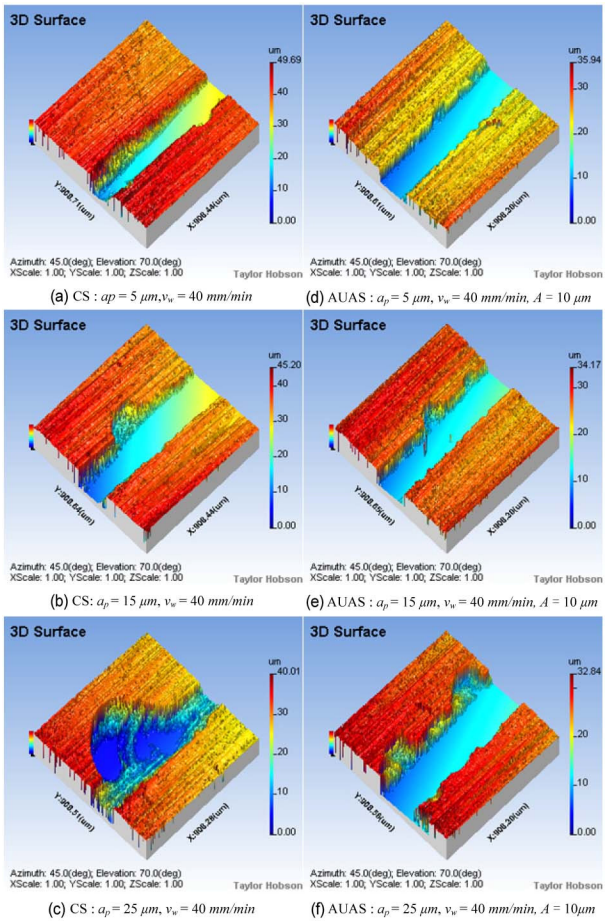

(a) CS : $ap = 5\ \mu m, v_w = 40\ mm/min$ (d) AUAS : $a_p = 5\ \mu m, v_w = 40\ mm/min, A = 10\ \mu m$

(b) CS: $a_p = 15\ \mu m, v_w = 40\ mm/min$ (e) AUAS : $a_p = 15\ \mu m, v_w = 40\ mm/min, A = 10\ \mu m$

(c) CS : $a_p = 25\ \mu m, v_w = 40\ mm/min$ (f) AUAS : $a_p = 25\ \mu m, v_w = 40\ mm/min, A = 10 \mu m$

Fig. 11. Comparison of the typical scratching morphologies.

brittle fracture in the AUAS is far less than that in the CS. This is because the normal grinding force and grinding force ratio under the effects of the axial ultrasonic vibration are smaller than those in the CS, which reduce the friction between the abrasive and the workpiece and facilitate the material removal process. Therefore, the quality of the surface grooves is better than that in the CS.

4.3 Analyses of the subsurface crack morphology

Fig. 12 displays the crack morphology of the subsurface in the different grinding methods. Fig. 12(a) shows that the subsurface cracks in the CS are primarily deep median cracks, whose direction changes as their propagation depths increase. Fig. 12(b) presents that the subsurface cracks of the machined surface under the AUAS are primarily shallow lateral micro-cracks. This is because the AUAS is a grinding method with a large tangential force and a small normal force. Moreover, the normal grinding force and grinding force ratio in the AUAS are smaller than those in the CS, which promotes the formation of lateral micro-cracks and inhibits the formation and propagation of median cracks. Therefore, the depth of the SSD in the AUAS

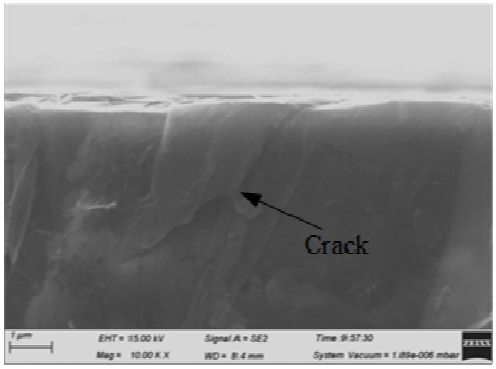

(a) CG (v_w = 13 m/s, a_p = 10 μm, A = 10 μm)

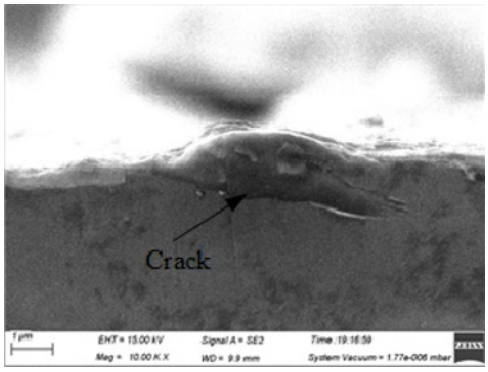

(b) AUAG (v_w = 13 m/s, a_p = 10 μm, A = 10 μm)

Fig. 12. Comparison of the subsurface crack morphologies.

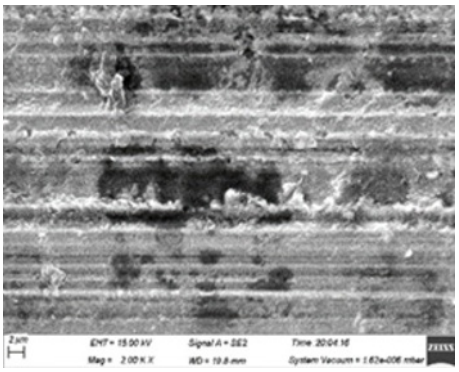

(a) CG (v_w = 13 m/s, a_p = 10 μm)

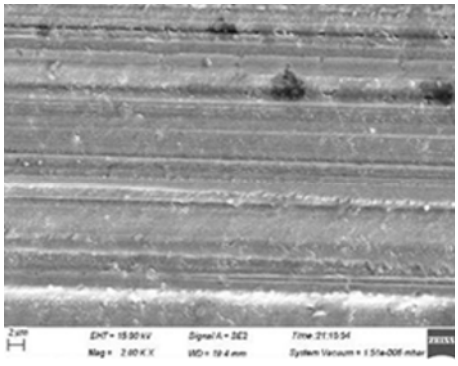

(b) AUAG (v_w = 13 m/s, a_p = 10 μm, A = 10 μm)

Fig. 13. Surface morphology (2000×).

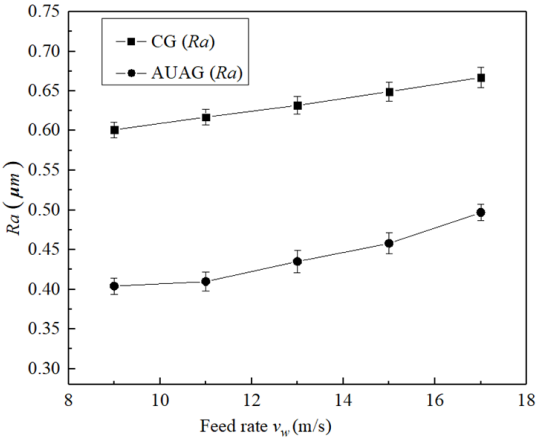

(a)

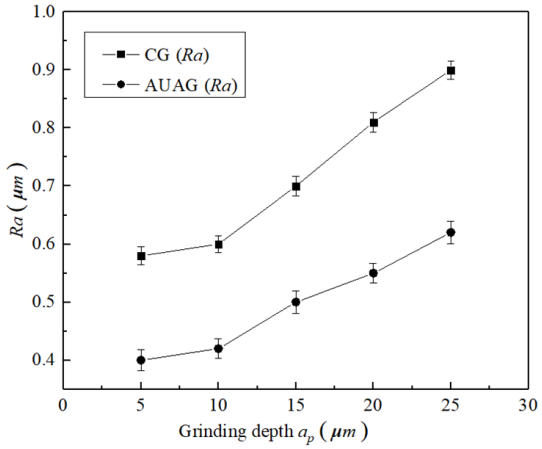

(b)

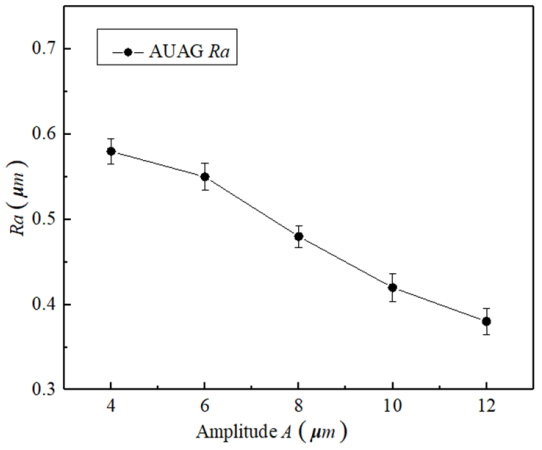

(c)

Fig. 14. The SR of nano-ZrO_2.

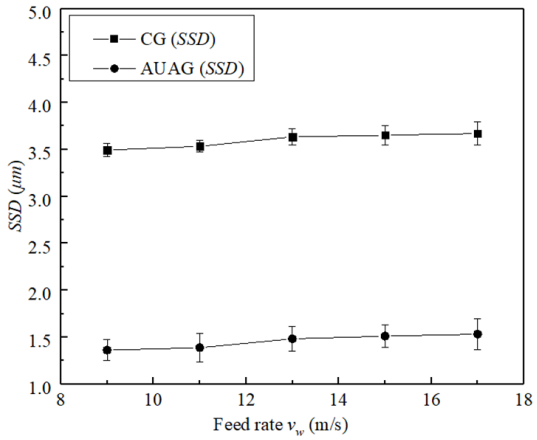

(a)

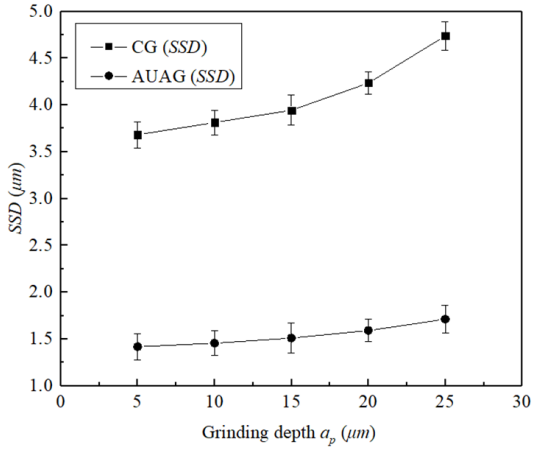

(b)

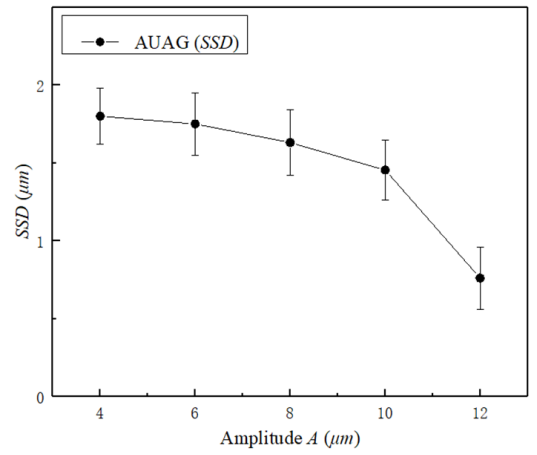

(c)

Fig. 15. The maximum SSD depth of nano-ZrO_2.

is comparatively shallower, and the subsurface cracks of the machined surface are primarily lateral micro-cracks.

Fig. 13 displays a comparison of the surface morphologies in the different processing methods. According to Fig. 13, under the same process parameters, the surface morphology in the CG presents a large area of block-like shedding, whereas in the AUAG, brittle fracture of the machined surface is observed and remarkable bulges are present on both sides of the grinding groove. The surface in the AUAG mainly exhibits plastic slipping. This is because under the same processing conditions, the UCT in the AUAG is reduced, so that the MRV under the mode of plastic deformation increases. In addition, the grinding

force model and surface crack morphology demonstrate the AUAG is a machining method with a large tangential force and a small normal force, which can effectively promote the formation and expansion of lateral micro-cracks. Moreover, the interference between the numerous lateral micro-cracks reduces the chip size, thereby improving surface quality.

Figs. 14 and 15 respectively depict the change rules of the SR and maximum SSD depth of nano-ZrO_2 in the AUAG and CG processes. It can be seen that both the properties increase with the feed rate and grinding depth; however, those in the AUAG are significantly smaller than those in the CG. This is because during the AUAG, the interference degree of the abrasive trajectory is greater than that in the CG, which reduces the UCT. Therefore, the surface quality in the AUAG is better than that in the CG. Moreover, the normal grinding force in the AUAG is smaller than that in the CG; therefore, the depths of the subsurface cracks are shallow. In addition, the AUAG is a processing method with large tangential and small normal forces, and the tangential grinding force presents a continuous high-frequency change due to the axial ultrasonic vibration, which affects the grinding surface, thus promoting the generation and propagation of lateral micro-cracks. The interference between the lateral micro-cracks reduces the SR.

According to Figs. 14(c) and 15(c), the SR and the maximum SSD depth decrease significantly with the vibration amplitude. This is becaupse the interference degree of adjacent cutting trajectories increases with the vibration amplitude, which decreases the sizes of chips, thereby improving the surface quality. On the other hand, because the grinding force needed to remove the material decreases with the vibration amplitude, the SR and the maximum SSD depth reduce with the vibration amplitude.

In summary, the AUAG is a processing method with large tangential and small normal forces, which are beneficial for material removal and can effectively improve surface quality.

5. Conclusion

Summarising, AUAG is a grinding method with a large tangential force and a small normal force, which can improve the surface integrity; therefore, it is suitable for the precision and ultra-precision machining of nano-ZrO_2 ceramics and other hard–brittle materials. The main conclusions are as follows:

1) The model of the UCT was established according to the cutting model of a single particle in AUAG. This model indicated that the UCT of a single particle in AUAG decreases significantly. Therefore, the material removal volume based on the removal modes of toughness is larger and the workpiece surface quality can be significantly improved during AUAG.

2) The models of the grinding force and grinding force ratio in AUAG were established based on the kinematic analysis and the UCT of a single particle. The analysis found that the grinding force and the grinding force ratio were significantly smaller than those in CG, and AUAG was a machining method with a large tangential force and a small normal force, which in turn promotes the removal of hard-brittle materials and reduces the degree of subsurface damage.

3) The nano-ZrO_2 ceramic grinding experiments indicated that the SR and maximum SSD depth of nano-ZrO_2 ceramic in the AUAG were significantly smaller than those in the CG, which is consistent with the theoretical analysis. The research provides a new idea for the study of surface and subsurface damage mechanism of hard-brittle materials in AUAG.

Acknowledgments

This research was sponsored by the National Natural Science Foundation of China (No. 51575163), Henan Polytechnic University Doctor Foundation project (No. B2010-76).

Nomenclature

A : Ultrasonic amplitude
f : Ultrasonic frequency
v_w : Feed rate of workpiece
v_s : Linear velocity of grinding
R : Grinding wheel radius
a_p : Temperature or Celsius temperature scale
E : Elastic modulus
h_i : The UCT
h_m : The maximum UCT
$\overline{h}$: The average UCT
K_{ID} : Dynamic fracture toughness
K_{IC} : Static fracture toughness
H_V : Vickers hardness
C_h : The depth of the lateral crack
C_l : The length of a lateral crack
C_m : The depth of the median crack
N_d : Dynamic distribution density of grains per area
N : The number of active grains per area
F_P : The main cutting force acting on a unit cutting area
p : The average contact pressure between the worn surface and the workpiece
F_{gt}, F_{gn} : The tangential grinding force and the normal grinding force in CG
F_{tc}, F_{nc} : The tangential force and the normal force generated by the cutting deformation
F_{ts}, F_{ns} : The tangential force and the normal force generated by friction
F_T, F_N : The tangential grinding force and the normal grinding force in AUAG
F_{tu}, F_{nu} : The tangential force and the normal force of the periodic pulse force.
K_F : The grinding force ratio in AUAG

Greek letters

ω_s : Grinding wheel angular speed
ω : Angular frequency of the workpiece
φ : Initial phase of the ultrasonic vibration

θ : Half-apex angle of particle
υ : Poisson's ratio
σ_y : Yield stress
β : Material parameter determined by elastic recovery
δ : The top area of a particle
μ : Friction coefficient

Acronyms and abbreviations

UAG : Ultrasonic-assisted grinding
AUAG : Axial ultrasonic-assisted grinding
SSD : Subsurface damage
CG : Conventional grinding
UCT : Undeformed chip thickness
UAST : Ultrasonic-assisted scratch test

References

[1] L. L. Wan et al., Thermal-mechanical coupling simulation and experimental research on the grinding of zirconia ceramics, *Journal of Manufacturing Processes*, 47 (2019) 41-51.
[2] R. Wdowik, J. Porzycki and M. Magdziak, Measurements of surface texture parameters after ultrasonic assisted and conventional grinding of ZrO_2 based ceramic material characterized by different states of sintering, *Procedia CIRP*, 62 (2017) 293-298.
[3] D. Zhang et al., Grinding model and material removal mechanism of medical nanometer zirconia ceramics, *Recent Patents on Nanotechnology*, 8 (1) (2014) 2.
[4] G. F. Gao et al., Research on the surface characteristics in ultrasonic grinding nano-zirconia ceramics, *Journal of Materials Processing Technology*, 209 (1) (2009) 32-37.
[5] J. Lopes et al., Application of MQL technique using TiO_2 nanoparticles compared to MQL simultaneous to the grinding wheel cleaning jet, *The International Journal of Advanced Manufacturing Technology*, 106 (5-6) (2020) 2205-2218.
[6] A. Talon et al., Effect of hardened steel grinding using aluminum oxide wheel under application of cutting fluid with corrosion inhibitors, *The International Journal of Advanced Manufacturing Technology*, 104 (1-4) (2019) 1437-1448.
[7] H. Wang et al., A mechanistic model on feeding-directional cutting force in surface grinding of CFRP composites using rotary ultrasonic machining with horizontal ultrasonic vibration, *International Journal of Mechanical Sciences*, 155 (2019) 450-460.
[8] D. Liu et al., A cutting force model for rotary ultrasonic machining of brittle materials, *International Journal of Machine Tools and Manufacture*, 52 (1) (2012) 77-84.
[9] E. Uhlmann and G. Spur, Surface formation in creep feed grinding of advanced ceramics with and without ultrasonic assistance, *CIRP Annals - Manufacturing Technology*, 47 (1) (1998) 249-252.
[10] Z. Liang et al., A new two-dimensional ultrasonic assisted grinding (2D-UAG) method and its fundamental performance in monocrystal silicon machining, *International Journal of Machine Tools and Manufacture*, 50 (8) (2010) 728-736.
[11] Z. Liang et al., Experimental study on brittle-ductile transition in elliptical ultrasonic assisted grinding (EUAG) of monocrystal sapphire using single diamond abrasive grain, *International Journal of Machine Tools and Manufacture*, 71 (2013) 41-51.
[12] D. Liu et al., A cutting force model for rotary ultrasonic machining of brittle materials, *International Journal of Machine Tools and Manufacture*, 52 (1) (2012) 77-84.
[13] C. Zhang, P. Feng and J. Zhang, Ultrasonic vibration-assisted scratch-induced characteristics of C-plane sapphire with a spherical indenter, *International Journal of Machine Tools and Manufacture*, 64 (2013) 38-48.
[14] C. Li et al., Material removal mechanism and grinding force modelling of ultrasonic vibration assisted grinding for SiC ceramics, *Ceramics International*, 43 (3) (2017) 2981-2993.
[15] M. Baraheni and S. Amini, Predicting subsurface damage in silicon nitride ceramics subjected to rotary ultrasonic assisted face grinding, *Ceramics International*, 45 (8) (2019) 10086-10096.
[16] Y. Wang et al., Study on the system matching of ultrasonic vibration assisted grinding for hard and brittle materials processing, *International Journal of Machine Tools and Manufacture*, 77 (2014) 66-73.
[17] Z. Yang et al., The grinding force modeling and experimental study of ZrO_2 ceramic materials in ultrasonic vibration assisted grinding, *Ceramics International*, 45 (7) (2019) 8873-8889.
[18] W. Gu, Z. Yao and H. Li, Investigation of grinding modes in horizontal surface grinding of optical glass BK7, *Journal of Materials Processing Tech.*, 211 (10) (2011) 1629-1636.
[19] T. G. Bifano and S. C. Fawcett, Specific grinding energy as an in-process control variable for ductile-regime grinding, *Precision Engineering*, 13 (4) (1991) 256-262.
[20] B. Zhao and B. M. Li, *Modern Grinding Technology*, 1st Ed., China Machine Press, Beijing, China (2003) 30-34.

Yanyan Yan is currently working at Henan Polytechnic University as an Associate Professor and a Master Tutor. She obtained a Doctor's degree from School of Mechanical Engineering, Shanghai Jiao Tong University in 2009, and mainly is engaged in scientific research work, such as precision processing and ultra-precision processing of hard-brittle materials, advanced manufacturing technology and precision machining equipment, etc.

Yafei Zhang is a Master of the School of Mechanical and Power Engineering, Henan Polytechnic University. She obtained a Bachelor's degree from this University in 2018. Her research interests include precision processing and ultra-precision processing of hard-brittle materials, ultrasonic assisted processing, etc.